Bidirectional Selector Realized Through Multilayer Tunnel Barrier Engineering

DEQUAN DONG[1], HUIKAI HE[1], JIAN XIA[1], RUI YANG [2,3], AND XIANGSHUI MIAO [2,3], (Senior Member, IEEE)

1 State Key Laboratory of Material Processing and Die & Mould Technology, School of Material Science and Engineering,
Huazhong University of Science and Technology, Wuhan 430074, China
2 Hubei Yangtze Memory Laboratories, Wuhan 430205, China
3 Wuhan National Laboratory for Optoelectronics, School of Optical and Electronic Information, School of Integrated Circuits,
Huazhong University of Science and Technology, Wuhan 430074, China

CORRESPONDING AUTHOR: R. YANG (e-mail: yangrui@hust.edu.cn)

ABSTRACT The selector plays an important role in solving the leakage current issue in a large-scale memory crossbar array. Especially, the bidirectional selector has a broader application scope than the unidirectional one, since it can be connected with both unipolar and bipolar memory devices. In this letter, two engineering approaches to realize bidirectional tunneling barrier selectors were investigated: the crested barrier and variable oxide thickness (VARIOT). It is found that the selectors based on the crested barrier exhibit much higher nonlinearity and lower off-current than those fitting the VARIOT approach. The associated tunneling mechanisms have been proposed to explain the electrical properties of the crested barrier devices. The excellent multilayer barrier bidirectional selector has been realized in the $ZnO/Ta_2O_5/ZnO$ stack with pA-level off current and high nonlinearity ($>10^4$). It is worth noting that the present $ZnO/Ta_2O_5/ZnO$ selector shows the best performances compared with previously reported tunnel barrier selectors.

INDEX TERMS Bidirectional selector, crested barrier, high nonlinearity, multilayer tunnel barrier.

I. INTRODUCTION

The crossbar array allows the smallest feature size of $4F^2$ and three-dimensional stacking to achieve high-density integration. In a crossbar array, resistive random access memory (RRAM) can be integrated at the junctions of orthogonal access lines that may enable n-layer stacking or the vertical fabrication of 3D crossbar arrays, which has attracted considerable attention for the physical demonstration of next-generation memory and computing centers [1]–[3].

However, as all cells in a row and column are connected to each other by the bottom and top electrode, the sneak current through neighboring units is still a bottleneck problem, which induces misreading and increasing power consumption in the crossbar array [4], [5]. Owing to the increasing number of sneak current paths in high-density integration, the selector device becomes indispensable. To effectively suppress the sneak current, the selector device

was required to realize high nonlinearity and ultralow off-current, as shown in Fig. 1(a). The sneak current paths can be suppressed due to their nonlinear current-voltage (*I-V*) characteristics. Since a bidirectional selector has better device uniformity and endurance than a unidirectional device, it is better suited to realize a cross-point array with a $4F^2$ cell for high density nonvolatile memory applications. In a commercial high-density memory system such as DRAM, a Si-based transistor is employed as a selector. However, the use of this three-terminal transistor in crossbar RRAM is limited due to its high expense of scaling down and stacking up [1]. Therefore, much effort has been dedicated towards developing various two-terminal bidirectional selectors, including Ovonic Threshold Switching (OTS) Selector [6], [7], Metal-Insulator-Transition (MIT) device [8], [9], Mixed-Ion-Electronic-Conduction (MIEC) based selector [10], timing selector [35], and tunnel barrier selector [3], [11], [12]. However, an ideal selector is yet to be demonstrated,

especially the off state current, cycling endurance, and the device to device variation are still need to be improved to meet the requirements in practical applications. Among them, the tunnel barrier selector has been one of the most promising candidates due to its outstanding durability and uniformity compared with other selectors, since it involves only electron transport and no ion migration during operation [13], [36], [37].

Two approaches of multilayer barrier engineering were proposed to increase the nonlinearity of the device. In 1998, Likharev first developed the concept of crested barrier, in which "crested" potential profile peaks in the middle layer [14]. To form a triangular-like potential barrier, sandwich a dielectric layer with a smaller electron affinity (usually larger bandgap) between two dielectric layers with a larger electron affinity (usually smaller bandgap), see Fig. 1(b). This designed barrier is much more sensitive to the applied voltage than the uniform barrier, resulting in high nonlinearity [15]. In contrast, variable oxide thickness (VARIOT) is the other barrier modulation approach [16], where the device has the configuration of the low-k (dielectric constant k) layer/high-k layer/low-k layer, as shown in Fig. 1(c). It is proposed that the electric field will redistribute and accumulate in the low-k layer, thus the equivalent barrier thickness reduces and results in steep tunnel current-voltage characteristics, which enhances the nonlinearity of the device [17]. Generally, the semiconductor with low/high k has a large/small bandgap, and vice versa [18], [21]. Thus, the device configuration of the VARIOT approach is opposite to that of the crested barrier. Which approach is much suitable for the selector design? To the best of our knowledge, there is no report about this till now.

In this work, several multilayer devices based on binary oxides (e.g., ZnO, Ta_2O_5, and HfO_2) have been prepared according to the crested barrier and VARIOT approaches. Experimental results directly indicate the devices based on identical materials but different approaches show completely different performances. The crested barrier approach is much more effective than the VARIOT approach in realizing high nonlinearity and low-leak current. An excellent selector of $ZnO/Ta_2O_5/ZnO$ stacking was obtained based on the crested barrier, showing ultralow leakage current ($\sim$pA level), symmetric and high nonlinearity ($>10^4$), good durability, and immunity to read disturbance. Through the investigation of electrical transport mechanisms of the crested barrier devices, it is found that this outstanding performance originates from Fowler-Nordheim (FN) tunneling.

II. EXPERIMENT

The multilayer tunnel barrier selector devices were fabricated on a Si substrate with 500 nm-thick SiO_2. Various binary oxide films were deposited by magnetron sputtering at room temperature from oxide targets. Fig. 1(b) shows the schematic structure of the crested barrier device, the thickness of the oxide layer is 8 nm for the outer layer and 4 nm
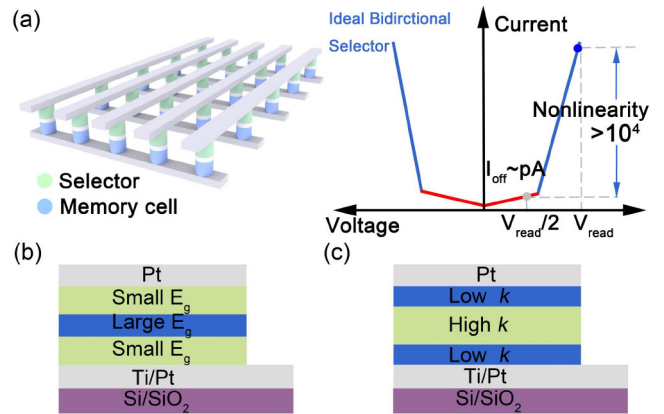

FIGURE 1. (a) Schematic of the crossbar with one selector-one memory unit. The ideal bidirectional selector device requires strong leakage current suppression capability and high nonlinearity. Schematic diagram of the two approaches for multilayer barrier engineering: (b) crested barrier and (c) VARIOT.

TABLE 1. Stack structure and thick parameters of crested barrier and VARIOT.

Crested barrier			VARIOT		
C1	$WO_3/HfO_2/WO_3$		V1	$HfO_2/WO_3/HfO_2$	
C2	$ZnO/HfO_2/ZnO$		V2	$Ta_2O_5/WO_3/Ta_2O_5$	
C3	$ZnO/Ta_2O_5/ZnO$	8/4/8 nm	V3	$CeO_2/Nb_2O_5/CeO_2$	4/8/4 nm
C4	$Nb_2O_5/Ta_2O_5/Nb_2O_5$		V4	$Ta_2O_5/Nb_2O_5/Ta_2O_5$	
C5	$ZnO/CeO_2/ZnO$		V5	$HfO_2/Nb_2O_5/HfO_2$	

for the middle layer. In contrast, the out layer is 4 nm and the middle layer is 8 nm for the VARIOT device, as shown in Fig. 1(c). And, to investigate the layer thickness dependence of nonlinearity, two VARIOT devices with different thickness configurations of 8/4/8 nm and 8/6/8 nm were prepared too. Both bottom and top Pt electrodes were prepared by sputtering and patterned via shadow masks with a size of 60 μm $\times$ 60 μm. Table 1 shows the stacked structure and thickness parameters of all prepared devices.

Electrical characterization was performed by DC voltage sweeping, using the Keithley 4200-SCS Semiconductor Parameter Analyzer (SPA) connected with a probe station (Cascade SUMMIT 11000B). For the pulse test, a Keysight B1530A Waveform Generator/Fast Measurement Unit was used to generate the voltage pulse and measure the current. During electrical measurement, the bottom electrode was grounded and the bias was applied on the top electrode.

III. RESULTS AND DISCUSSION

The conduction band of the crested barrier is schematically shown in Fig. 2(a). The outer flat lines represent the work function of the metal electrode (e.g., Pt, Au) while the inner ones represent the conduction band of dielectric oxides. The dotted line approximates the effective band offset when a voltage V is applied. In the device with a homogeneous or "square" barrier (up panel in Fig. 2(a)), electrons travel through an effective triangular barrier under an external electrical field. Compared with a single-layer barrier, the height and width of the crested barrier are reduced under high
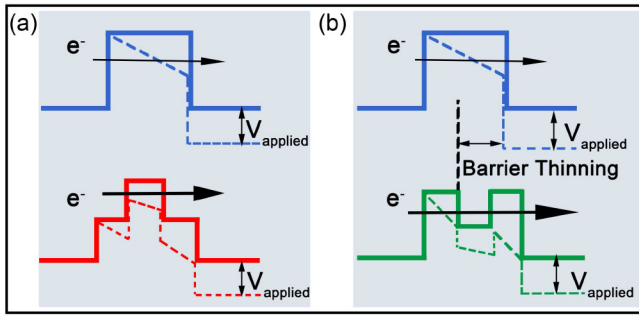
FIGURE 2. The schematic diagram of the single and tri-layer barrier: (a) Crested Barrier and (b) Variable Oxide Thickness. The solid lines represent a homogeneous or "square" barrier. The dotted lines show the barrier tilting caused by the applied voltage.

TABLE 2. Experimental bandgap, electron affinity, and dielectric constant of the candidate tunnel barrier materials.

Materials	Bandgap/eV	Electron affinity/eV	Dielectric constant	Refs.
ZnO	3.4	4.5	8.6	[19], [20]
Ta_2O_5	4.4	3.3	22	[21], [22]
HfO_2	5.8	2.2	25	[21], [23]
Nb_2O_5	3.44	3.87	38	[24], [25]
WO_3	3.28	4.1	50	[26], [27]
CeO_2	3.15	3.5	26	[28], [29]

voltage, see the bottom panel of Fig. 2(a) [13]. In this case, when a voltage is applied, the overall barrier height that the electrons encounter is shorter (and effectively thinner for tunneling electrons) and resulting in a high nonlinearity. Fig. 2(b) shows a schematic diagram of VARIOT. The electric field applied on the multilayer stack will be redistributed, resulting in barrier thinning compared to the single-layer barrier. Theoretically, both the crested barrier and VARIOT can increase the nonlinearity of the device. To explore which one is much more effective, we symmetrically combined some widely used binary oxides to form tri-layer barriers, including ZnO, Ta_2O_5, HfO_2, Nb_2O_5, WO_3, and CeO_2. The physical parameters of these candidate materials are reported in Table 2. More than 10 multilayer devices were prepared with half following the crested barrier and half falls in VARIOT approach.

As shown in Fig. 3(a), in the case of the crested barrier ZnO/Ta_2O_5/ZnO (C3) device performs strong current suppression characteristics at a voltage less than 1 V. The device is almost insulated, with a current of 1.2×10^{-11} A at 1 V, but the current rapidly increases to 3×10^{-5} A at 3 V, inducing excellent nonlinear characteristics. It is noteworthy that this device performs symmetric *I-V* nonlinearity, which is indispensable to block current flow in both directions at low voltage magnitudes. The ZnO/HfO_2/ZnO (C2) device also shows comparable nonlinear performance to the ZnO/Ta_2O_5/ZnO device, however, its off-state resistance is lower, resulting in an increase of leakage current. The other three devices, i.e., Nb_2O_5/Ta_2O_5/Nb_2O_5 device (C4), WO_3/HfO_2/WO_3 device (C1), and ZnO/CeO_2/ZnO device (C5), perform much lower off-state resistance at low voltage,
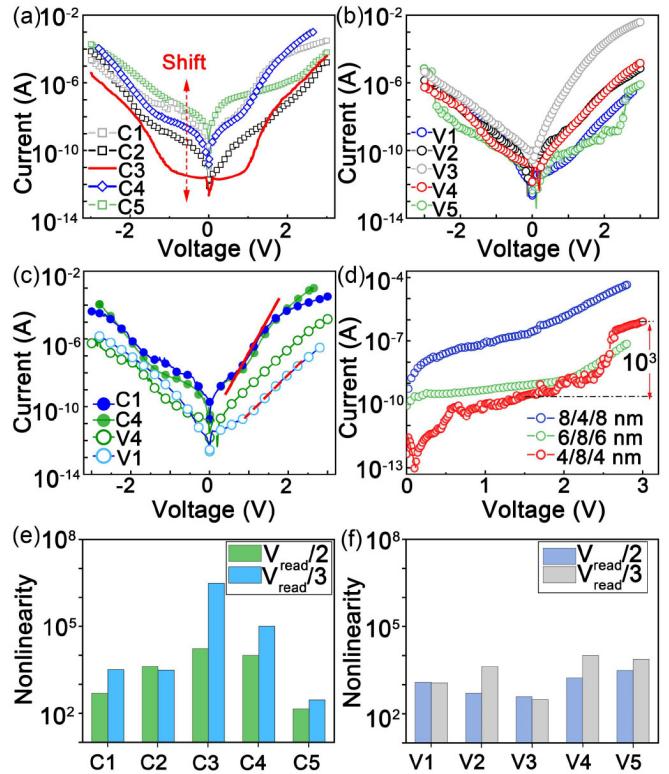

FIGURE 3. *I-V* characteristics of the device with the crested barrier (a) labels C1, C2, C3, C4, and C5 are the crested barrier device WO_3/HfO_2/WO_3, ZnO/HfO_2/ZnO, ZnO/Ta_2O_5/ZnO, Nb_2O_5/Ta_2O_5/Nb_2O_5, and ZnO/CeO_2/ZnO, respectively and VARIOT (b), labels V1, V2, V3, V4, and V5 are the VARIOT device HfO_2/WO_3/HfO_2, Ta_2O_5/WO_3/Ta_2O_5, CeO_2/Nb_2O_5/CeO_2, Ta_2O_5/Nb_2O_5/Ta_2O_5, and HfO_2/Nb_2O_5/HfO_2, respectively, dotted line with an arrow works as a guide to the eye in panel (a). (c) *I-V* curves of four devices with the same materials but with different morphology according to the crested barrier (filled circle) and VARIOT (hollow circle). (d) The effect of each layer thickness on the nonlinearity for the HfO_2/Nb_2O_5/HfO_2 devices: 8/4/8 nm, 6/8/6 nm, and 4/8/4 nm. The nonlinearity of the devices in accordance with (e) crested barrier and (f) VARIOT for two reading schemes.

resulting in sharply decrease of nonlinearity compared with the device of ZnO/Ta_2O_5/ZnO.

To prepare the tunnel barrier following the VARIOT approach, we reverse the arrangement of the material combination shown in Fig. 3(a). As shown in Fig. 3(b), all the VARIOT devices exhibit relatively lower nonlinearity compared with those crested barrier devices. To rule out the influence of materials on the device nonlinearity, two groups of devices with the same materials but opposite configurations are reported in Fig. 3(c). It is clearly seen that the crested barrier devices show a steeper *I-V* curve compared with that of the VARIOT device. Note that a higher Schottky barrier is usually formed at the Pt/oxides interfaces in the VARIOT compared with the crested barrier device based on the same materials. Take C1 (Pt/WO_3/HfO_2/WO_3/Pt) and V1 (Pt/HfO_2/WO_3/HfO_2/Pt) devices as an example, the Schottky barrier height of the Pt/HfO_2 (3.45 eV) interface is theoretically higher than the Pt/WO_3 (1.5 eV) interface, which might be resulting in the high resistance of the
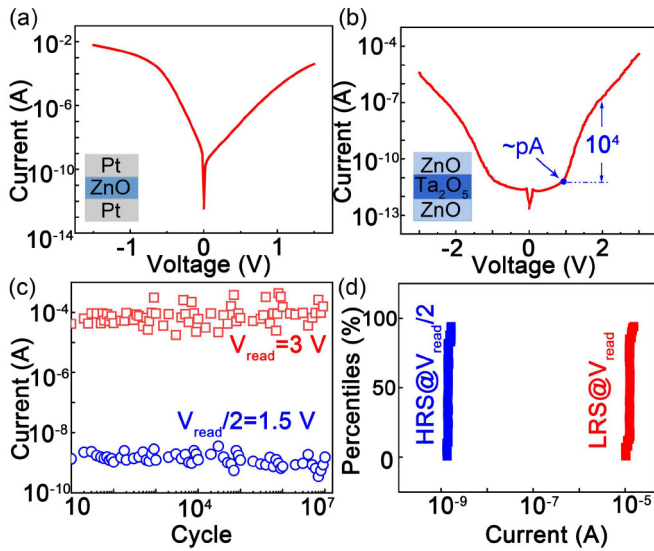
FIGURE 4. The *I-V* curve of the device based on (a) the single layer of ZnO and (b) the crested barrier of ZnO/Ta$_2$O$_5$/ZnO. (c) The pulse response of the ZnO/Ta$_2$O$_5$/ZnO stack by applying pulses of 3.0 V/1 ms and 1.5 V/1 ms. The nonlinearity of the device remains 10^7 during pulse cycles. (d) Cumulative probability of current at V$_{read}$ and V$_{read}$/2 schemes.

FIGURE 5. (a) Fowler-Nordheim tunneling fitting of ln (I/V^2) versus (1/|V|) for the device of ZnO/Ta$_2$O$_5$/ZnO. (b) Comparison of the nonlinearity versus off current and on current of reported tunnel barrier selector devices.

VARIOT devices. Thus it is reasonable that the *I-V* curve of the VARIOT device is several orders of magnitude lower than the ones with the crested barrier.

Furthermore, we count the nonlinearity of the crested barriers and VARIOT devices in the case of V$_{read}$/2 and V$_{read}$/3 schemes, results are shown in Fig. 3(e) and (f). These results clearly show that all the nonlinearity values of the crested barriers almost are higher than those of the VARIOT devices in both two reading schemes, indicating the crested barrier is more effective to obtain high nonlinearity. Our experimental results indicate the barrier height has a much more significant impact on the tunneling characteristics of the device than the dielectric constants of the materials. And, it is noticeable that the nonlinearity of the ZnO/Ta$_2$O$_5$/ZnO device reaches 3×10^6 for the V$_{read}$/3 scheme (3 V as V$_{read}$), which is comparable to the reported Ovonic threshold switching selector [6]. Given the thickness of each layer affects the nonlinearity of the VARIOT device [18], thus we prepared another two VARIOT devices of HfO$_2$/Nb$_2$O$_5$/HfO$_2$ with a thickness of each layer 8/4/8 nm and 6/8/6 nm. As shown in Fig. 3(d), the device with 4/8/4 nm thickness shows the best nonlinearity compared with another two devices, indicating a thinner outer layer facilitates the enhancement of the device's nonlinearity. But, this best nonlinearity valve is still not competitive with that of the crested barrier device.

In addition, a device based on a single ZnO layer was prepared for comparison with the ZnO/Ta$_2$O$_5$/ZnO device, results are shown in Fig. 4(a) and (b). The *I-V* curve of the single-layer ZnO device shows the performance of resistance, that is, the current increases linearly with the increase of voltage. This is because the highest point of the single-layer barrier hardly drops when a voltage is applied, thus
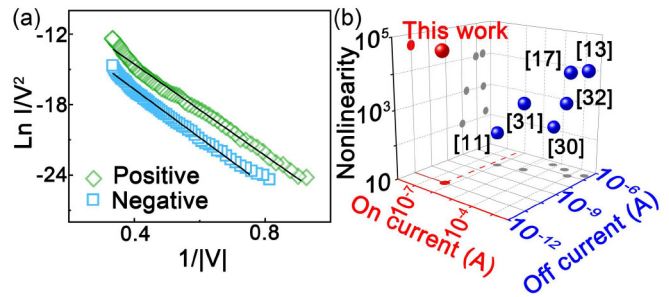
preventing electrons from passing through the barrier. In contrast, after adopting a symmetric stacked barrier structure, the *I-V* characteristic of the ZnO/Ta$_2$O$_5$/ZnO device shows high nonlinearity, directly indicating that the high nonlinearity originates from the crested barrier structure. And, the Off-current of this device drops below pA-level when setting the read voltage lower than 1 V. At the same time, this device shows symmetry *I-V* curves under positive and negative bias. This is because the height of the barriers of the top Pt/ZnO/Ta$_2$O$_5$ interfaces is almost the same as the bottom Ta$_2$O$_5$/ZnO/Pt interface. And, it has been reported that the asymmetry of the *I-V* curves decreases as the average height of the Schottky barrier increase based on theoretical calculations [33]. The ZnO/Ta$_2$O$_5$/ZnO device possesses a high Schottky barrier, thus it is reasonable it performs better symmetric *I-V* curves.

To evaluate the endurance of the crested device with ZnO/Ta$_2$O$_5$/ZnO stack, pulse pairs of 3.0 V/1 ms and 1.5 V/1 ms were applied to the device, the device response is shown in Fig. 4(c). The ON and OFF states show negligible deterioration during 10^7 pulse cycles, resulting in a high ON/OFF ratio ($>10^5$) and good endurance. And, the dc cycling voltage sweeping was also carried out, the cumulative probability of ON and OFF state is shown in Fig. 4(d). The device exhibits relatively narrow cycle-to-cycle variations indicating high stability of both ON and OFF states. These results clearly show the excellent endurance and uniformity of this crested barrier. The low ON/OFF variations and switching uniformity might be attributed to the effect of the barrier uniformity in the ZnO/Ta$_2$O$_5$/ZnO devices.

A comparison of our ZnO/Ta$_2$O$_5$/ZnO selector with other reported bidirectional tunnel barrier selectors, in terms of nonlinearity, on and off currents, is given in Fig. 5(b). The crested barrier of the ZnO/Ta$_2$O$_5$/ZnO device performs very competitive nonlinearity and leakage current, even though the on current ($\sim$10 μA) might need further enhancement for some memory devices. This pA-level off current and high nonlinearity ($>10^4$) are the best performances compared with previously reported tunnel barrier selectors. At the same time, the present ZnO/Ta$_2$O$_5$/ZnO selector possesses competitive endurance compared to the reported selectors [11], [38].
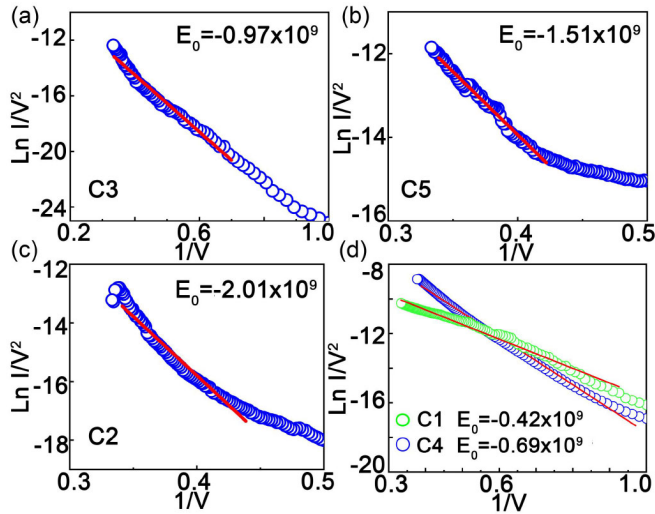
FIGURE 6. The Fowler-Nordheim plots for (a) C3 (ZnO/Ta$_2$O$_5$/ZnO), (b) C5 (ZnO/CeO$_2$/ZnO), (c) C2 (ZnO/HfO$_2$/ZnO), (d) C1 (WO$_3$/HfO$_2$/WO$_3$) and C4 (Nb$_2$O$_5$/Ta$_2$O$_5$/Nb$_2$O$_5$). The values of slope E$_0$ are listed for positive bias for each sample.

Following we will focus on the discussion of why the ZnO/Ta$_2$O$_5$/ZnO device performs the best nonlinearity compared with other four crested barrier devices. To investigate the conduction mechanism prevailing in the high field region of the crested devices, *I-V* curves have been fitted in both positive and negative bias regions. It has been found that the electrical transport processes of these crested devices fit FN tunneling when the voltage exceeds 1 V in both polarities, as shown in Fig. 5(a). The current density in FN tunneling is given by

$$\ln \frac{I}{V^2} = \ln \alpha - \frac{E_0 d}{V} \quad (1)$$

With

$$\alpha = \frac{S\pi m e^3}{d^2 k_1^2 h^3}$$

And

$$E_0 = -2\bar{k}\phi_b/e$$

where h is the Planck constant, m is the mass of a free electron, e is the charge of a single electron, S is the electrode area, d is the thickness of the dielectric material layer, k_1 is the value of the imaginary wave number at the injection interface, $\bar{k}$ is the average value of the imaginary wave number in the oxide barrier, and Φ_b is the energy barrier at the injection interface [34]. As shown in Equation (1), the FN tunnel current I is exponentially dependent on the applied field V. Plotting ln (I/V^2) versus 1/V, should yield a straight line with a slope that is related to the barrier height Φ_b. By plotting ln (I/V^2) versus 1/V from the *I-V* curves, we can induce the effective barrier height of a device by calculating the slope of $E_o d$, because the E_o values are directly proportional to the barrier height.

Fig. 6 shows the *I-V* plots and FN fitting results in the high voltage region (≥ 1 V) for the prepared five devices with

crested barrier. The deduced E_o values are reported in the insets. For the three devices with the same outer layer material of ZnO, as shown in Fig. 6(a), (b) and (c), the device of ZnO/Ta$_2$O$_5$/ZnO possesses the minimum absolute value of E_o, indicating the electron barrier lowers the most under high external bias. Thus, this device performs the most rapid current growth under a certain voltage, resulting in the highest on/off state ratio among these three devices. For another two devices of Nb$_2$O$_5$/Ta$_2$O$_5$/Nb$_2$O$_5$ and WO$_3$/HfO$_2$/WO$_3$, the absolute value of E_o is lower than that of the device of ZnO/Ta$_2$O$_5$/ZnO, which means the barrier lowering in these two devices are much stronger under high bias. However, the leakage current of these two devices under low voltage (<1 V) is two to three orders of magnitude higher than that of the ZnO/Ta$_2$O$_5$/ZnO device, resulting in a serious deterioration of the nonlinearity. Note that the Pt/Nb$_2$O$_5$ and Pt/WO$_3$ interfaces theoretically have a much higher Schottky barrier than the Pt/ZnO interface due to the lower electron affinity of Nb$_2$O$_5$ (3.87 eV) and WO$_3$ (4.10 eV) compared to ZnO (4.50 eV). This Schottky barrier of the interface might lower a lot under high bias, resulting in a low value of E_o in the device. The high leakage current of these two devices might result from relatively low effective thicknesses or several non-idealities formed at the Pt/oxides interfaces, which need further investigations.

IV. CONCLUSION

In summary, this work systematically investigates two multilayer barrier engineering approaches. It is found that the crested barrier approach is much more effective than the VARIOT one in improving the nonlinear performance of the multilayer barriers. And symmetric and high nonlinearity ($>10^4$) and pA-level leakage current were realized in the crested barrier of the ZnO/Ta$_2$O$_5$/ZnO device.

REFERENCES

[1] Q. Xia and J. J. Yang, "Memristive crossbar arrays for brain-inspired computing," *Nat. Mater.*, vol. 18, pp. 309–323, Mar. 2019, doi: 10.1038/s41563-019-0291-x.

[2] Y. Li and K.-W. Ang, "Hardware implementation of neuromorphic computing using large-scale memristor crossbar arrays," *Adv. Intell. Syst.*, vol. 3, no. 1, 2021, Art. no. 2000137, doi: 10.1002/aisy.202000137.

[3] Q. Luo *et al.*, "Highly uniform and nonlinear selection device based on trapezoidal band structure for high density nano-crossbar memory array, " *Nano. Res.*, vol. 10, no. 10, pp. 3295–3302, May 2017, doi: 10.1007/s12274-017-1542-2.

[4] J. J. Yang, D. B. Strukov, and D. R. Stewart, "Memristive devices for computing," *Nat. Nanotechnol.*, vol. 8, pp. 13–24, Dec. 2012, doi: 10.1038/nnano.2012.240.

[5] Y. Cassuto, S. Kvatinsky, and E. Yaakobi, "Sneak-path constraints in memristor crossbar arrays," in *Proc. IEEE Int. Symp. Inf. Theory*, Oct. 2013, pp. 156–160, doi: 10.1109/ISIT.2013.6620207.

[6] Y. Koo, S. Lee, S. Park, M. Yang, and H. Hwang, "Simple binary ovonic threshold switching material SiTe and its excellent selector performance for high-density memory array application," *IEEE Electron Device Lett.*, vol. 38, no. 5, pp. 568–571, May 2017, doi: 10.1109/LED.2017.2685435.

[7] M. J. Lee *et al.*, "A plasma-treated chalcogenide switch device for stackable scalable 3D nanoscale memory," *Nat. Commun.*, vol. 4, no. 2629, pp. 1–8, Sep. 2013, doi: 10.1038/ncomms3629.

[8] T.-H. Yeh *et al.*, "Enhancing threshold switching characteristics and stability of vanadium oxide-based selector with vanadium electrode," *IEEE Trans. Electron Devices*, vol. 67, no. 11, pp. 5059–5062, Nov. 2020, doi: 10.1109/TED.2020.3019773.

[9] M. Son *et al.*, "Excellent selector characteristics of nanoscale VO_2 for high-density bipolar ReRAM applications," *IEEE Electron Device Lett.*, vol. 32, no. 11, pp. 1579–1581, Nov. 2011, doi: 10.1109/LED.2011.2163697.

[10] Q. Luo *et al.*, "Super non-linear RRAM with ultra-low power for 3D vertical nano-crossbar arrays," *Nanoscale*, vol. 8, pp. 15629–15636, Jul. 2016, doi: 10.1039/c6nr02029a.

[11] J. Woo *et al.*, "Electrical and reliability characteristics of a scaled (~30 nm) tunnel barrier selector ($W/Ta_2O_5/TaO_x/TiO_2/TiN$) with excellent performance ($J_{MAX} > 10^7 A/cm^2$)," in *Proc. IEEE Symp. VLSI Technol.*, Sep. 2014, pp. 1–2, doi: 10.1109/VLSIT.2014.6894431.

[12] M. Wang, J. Zhou, Y. Yang, S. Gaba, M. Liu, and W. D. Lu, "Conduction mechanism of a TaO_x-based selector and its application in crossbar memory arrays," *Nanoscale*, vol. 7, no. 11, pp. 4964–4970, Feb. 2015, doi: 10.1039/C4NR06922F.

[13] B. J Choi *et al.*, "Trilayer tunnel selectors for memristor memory cells," *Adv. Mater.*, vol. 28, pp. 356–362. Jan. 2016, doi: 10.1002/adma.201503604.

[14] K. K. Likharev, "Layered tunnel barriers for nonvolatile memory devices," *Appl. Phys. Lett.*, vol. 73, no. 15, pp. 2137–2139. Aug. 1998, doi: 10.1063/1.122402.

[15] E. Cimpoiasu *et al.*, "Aluminum oxide layers as possible components for layered tunnel barriers," *J. Appl. Phys.*, vol. 96, no. 2, pp. 1–7, Jun. 2004, doi: 10.1063/1.1763229.

[16] B. Govoreanu, P. Blomme, M. Rosmeulen, J. V. Houdt, and K. D. Meyer, "VARIOT: A novel multilayer tunnel barrier concept for low-voltage nonvolatile memory devices," *IEEE Electron Device Lett.*, vol. 24, no. 2, pp. 99–101, Feb. 2003, doi: 10.1109/LED.2002.807694.

[17] W. Lee *et al.*, "High current density and nonlinearity combination of selection device based on $TaO_x/TiO_2/TaO_x$ structure for one selector-one resistor arrays," *ACS Nano*, vol. 6, no. 9, pp. 8166–8172, Aug. 2012, doi: 10.1021/nn3028776.

[18] J. D. Casperson, L. D. Bell, and H. A. Atwater, "Materials issues for layered tunnel barrier structures," *J. Appl. Phys.*, vol. 92, no. 1, pp. 261–267, Mar. 2002, doi: 10.1063/1.1479747.

[19] D. P. Norton *et al.*, "ZnO: Growth, doping & processing," *Mater. Today*, vol. 7, no. 6, pp. 34–40, Jun. 2004, doi: 10.1016/S1369-7021(04)00287-1.

[20] K. B. Sundaram and A. Khan, "Work function determination of zinc oxide films," *J. Vac. Sci. Technol. B*, vol. 15, no. 2, pp. 428–430, Jun. 1998, doi: 10.1116/1.580502.

[21] J. Robertson, "High dielectric constant oxides," *Eur. Phys. J. Appl. Phys.*, vol. 28, no. 3, pp. 265–291, Dec. 2004, doi: 10.1051/epjap:2004206.

[22] J. Robertson and C. W. Chen, "Schottky barrier heights of tantalum oxide, barium strontium titanate, lead titanate, and strontium bismuth tantalite," *Appl. Phys. Lett.*, vol. 74, no. 8, pp. 1168–1170, Feb. 1999, doi: 10.1063/1.123476.

[23] S. Monaghan, P. K. Hurley, K. Cherkaoui, M. A. Negara, and A. Schenk, "Determination of electron effective mass and electron affinity in HfO_2 using MOS and MOSFET structures," *Solid-State Electron.*, vol. 53, no. 4, pp. 438–444, 2009, doi: 10.1016/j.sse.2008.09.018.

[24] J. Jia *et al.*, "Visible and near-infrared photothermal catalyzed hydrogenation of gaseous CO_2 over nanostructured $Pd@Nb_2O_5$," *Adv. Sci.*, vol. 3, no. 10, pp. 1–13, Oct. 2016, doi: 10.1002/advs.201600189.

[25] S. Clima *et al.*, "Dielectric response of Ta_2O_5, $NbTaO_5$ and Nb_2O_5 from first-principles investigations," *ECS Trans.*, vol. 19, no. 2, pp. 729–737, 2009, doi: 10.1149/1.3122128.

[26] L. Weinhardt *et al.*, "Electronic surface level positions of WO_3 thin films for photoelectrochemical hydrogen production," *J. Phys. Chem. C*, vol. 112, no. 8, pp. 3078–3082, Feb. 2008, doi: 10.1021/jp7100286.

[27] Z. Zhou, Z. Wu, Q. Xu, and G. Zhao, "A solar-charged photoelectrochemical wastewater fuel cell for efficient and sustainable hydrogen production," *J. Mater. Chem. A.*, vol. 5, no. 48, pp. 25450–25459, Nov. 2017, doi: 10.1039/C7TA08112J.

[28] S. M. Yang, C. H. Chien, J. J. Huang, T. F. Lei, M. J. Tsai, and L. S. Lee, "Cerium oxide nanocrystals for nonvolatile memory applications," *Appl. Phys. Lett.*, vol. 91, no. 26, pp. 1–3, Dec. 2007, doi: 10.1063/1.2821367.

[29] M. Ismail *et al.*, "Effect of bilayer CeO_{2-x}/ZnO and ZnO/CeO_{2-x} heterostructures and electroforming polarity on switching properties of non-volatile memory," *Nanoscale Res. Lett.*, vol. 13, no. 318, pp. 1–10, Oct. 2018, doi: 10.1186/s11671-018-2738-4.

[30] A. Kawahara *et al.*, "An 8 Mb multi-layered cross-point ReRAM macro with 443 MB/s write throughput," in *Proc. IEEE Int. Solid-State Circuits Conf.*, Apr. 2012, pp. 432–434, doi: 10.1109/ISSCC.2012.6177078.

[31] B. Govoreanu, C. Adelmann, A. Redolfi, L. Zhang, S. Clima, and M. Jurczak, "High-performance metal-insulator-metal tunnel diode selectors," *IEEE Electron Device Lett.*, vol. 35, no. 1, pp. 63–65, Jan. 2014, doi: 10.1109/LED.2013.2291911.

[32] S. Lee, D. Lee, J. Woo, E. Cha, J. Park, and H. Hwang, "Engineering oxygen vacancy of tunnel barrier and switching layer for both selectivity and reliability of selector-less ReRAM," *IEEE Electron Device Lett.*, vol. 35, no. 10, pp. 1022–1024, Oct. 2014, doi: 10.1109/LED.2014.2347925.

[33] N. Tuomisto, A. Zugarramurdi, and M. J. Puska, "Modeling of electron tunneling through a tilted potential barrier," *J. Appl. Phys.*, vol. 121, Mar. 2017, Art. no. 134304, doi: 10.1063/1.4979533.

[34] J. D. Casperson, "Design and characterization of layered tunnel barriers for nonvolatile memory applications," Ph.D. dissertation, Dept. Electr. Eng., California Inst. Technol. Univ., Pasadena, CA, USA, 2004.

[35] M. Rao *et al.*, "Timing selector: Using transient switching dynamics to solve the sneak path issue of crossbar arrays," *Small Sci.*, vol. 1, no. 1, 2022, Art. no. 2100072, doi: 10.1002/smsc.202100072.

[36] N. K. Upadhyay *et al.*, "Engineering tunneling selector to achieve high non-linearity for 1S1R integration," *Front. Nanotechnol.*, vol. 3, pp. 28–38, Apr. 2021, doi: 10.3389/fnano.2021.656026.

[37] N. K. Upadhyay *et al.*, "A memristor with low switching current and voltage for 1S1R integration and array operation," *Adv. Electron. Mater.*, vol. 6, May 2020, Art. no. 1901411, doi: 10.1002/aelm.201901411.

[38] L. Zhang *et al.*, "High-drive current ($>1MA/cm^2$) and highly nonlinear ($>10^3$) TiN/amorphous-Silicon/TiN scalable bidirectional selector with excellent reliability and its variability impact on the 1S1R array performance," in *IEDM Tech. Dig.*, Dec. 2014, pp. 6.8.1–6.8.4, doi: 10.1109/IEDM.2014.7047000.